



1 **Ecosystem fluxes of carbonyl sulfide in an old-growth forest: temporal dynamics**  
2 **and responses to diffuse radiation and heat waves**

3 Bharat Rastogi<sup>1</sup>, Max Berkelhammer<sup>2</sup>, Sonia Wharton<sup>3</sup>, Mary E Whelan<sup>4</sup> Frederick C.  
4 Meinzer<sup>5</sup>, David Noone<sup>6</sup>, and Christopher J. Still<sup>1</sup>

5  
6 <sup>1</sup> Department of Forest Ecosystems and Society, Oregon State University, OR 97331,  
7 USA

8 <sup>2</sup> Department of Earth and Environmental Sciences, University of Illinois at Chicago,  
9 Chicago, Illinois, USA

10 <sup>3</sup> Atmospheric, Earth and Energy Division, Lawrence Livermore National Laboratory,  
11 7000 East Avenue, L-103, Livermore, CA 94550, USA

12 <sup>4</sup> Carnegie Institution for Science, 260 Panama St., Stanford, CA, USA, 94305

13 <sup>5</sup> USDA Forest Service, PNW Research Station, Corvallis, OR 97331, USA

14 <sup>6</sup> College of Earth, Ocean and Atmospheric Sciences, Oregon State University, OR  
15 97331, USA

16  
17 Corresponding author: Bharat Rastogi ([bharat.rastogi@oregonstate.edu](mailto:bharat.rastogi@oregonstate.edu))  
18

19 **Abstract**

20 Carbonyl sulfide (OCS) has recently emerged as a tracer for terrestrial carbon uptake.  
21 While physiological studies relating OCS fluxes to leaf stomatal dynamics have been  
22 established at leaf and branch scales and incorporated in global carbon cycle models, the  
23 quantity of data from ecosystem-scale field studies remains limited. In this study we  
24 employ established theoretical relationships to infer ecosystem-scale OCS uptake from  
25 concentration measurements. OCS uptake was found to scale with independent  
26 measurements of CO<sub>2</sub> fluxes over a 60-m-tall old-growth forest in the Pacific  
27 Northwestern U.S. (45°49'13.76" N; 121°57'06.88") at hourly and monthly timescales  
28 across the growing season in 2015. OCS fluxes tracked changes in soil moisture, and  
29 were strongly influenced by the fraction of downwelling diffuse light. Fluxes were also  
30 strongly affected by sequential heat waves during the growing season. Our results bolster  
31 previous evidence that ecosystem OCS uptake is strongly related to stomatal dynamics,  
32 and measuring this gas improves constraints on estimating photosynthetic rates at the  
33 ecosystem scale.

34  
35 **1. Introduction**

36 Carbonyl Sulfide (OCS) is the most abundant sulfur gas in the atmosphere, with a mean  
37 atmospheric concentration of ~500 ppt (parts per trillion), and therefore a significant part  
38 of the tropospheric and stratospheric sulfur cycles, with implications for the global  
39 radiation budget and ozone depletion (Johnson et al., 1993; Notholt et al., 2003). The  
40 dominant sink of atmospheric OCS is vegetation (Kesselmeier and Merk, 1993; Kettle et  
41 al., 2002; Montzka et al., 2007 and references therein), through rapid and irreversible  
42 hydrolysis by the ubiquitous enzyme carbonic anhydrase (Protoschill-Krebs, Wilhelm, &



43 Kesselmeier, 1996; Protoschill-Krebs and Kesselmeier, 1992). Recent advances in  
44 spectroscopic technology have enabled continuous in-situ measurements of OCS on  
45 timescales that are relevant to understanding stomatal function at the leaf-scale (Stimler  
46 et al., 2010a, 2010b), branch scale (Berkelhammer et al., 2014) and the ecosystem scale  
47 (Kooijmans et al., 2017; Wehr et al., 2017). An important distinction between OCS and  
48 CO<sub>2</sub> cycling is that there are no reported emissions from actively photosynthesizing  
49 leaves. However, the normalized leaf uptake ratio of OCS:CO<sub>2</sub> (LRU; Sandoval-Soto et  
50 al., 2005) is relatively constant at medium to high light levels (Maseyk et al., 2014;  
51 Stimler et al., 2010), making it an excellent proxy for quantifying plant productivity  
52 (GPP; Asaf et al., 2013; Billesbach et al., 2014; Blonquist et al., 2011). On the other  
53 hand, both uptake and emissions of OCS from soils have been identified (Whelan et al.,  
54 2016; Sun et al., 2015; Maseyk et al., 2014; Kesselmier et al., 1999). While ecosystem-  
55 scale measurements of OCS continue to establish links between OCS uptake and GPP in  
56 different ecosystems (for a comprehensive list of ecosystem scale studies readers are  
57 referred to Figure 2 in Whelan et al., 2017), inconsistencies persist. For example, in an  
58 oak-savanna woodland in southern France Belviso et al. (2016) found that OCS exchange  
59 was strongly influenced by photosynthesis during early morning hours, while meaningful  
60 values of LRU could only be calculated for a few days in the early afternoons. Commane  
61 et al. (2015) were unable to explain mid-summer emissions of OCS at a mid-latitude  
62 deciduous forest. Uncertainties highlighted above argue for field-scale measurements of  
63 OCS in a variety of ecosystems, particularly as OCS flux predictions have recently been  
64 incorporated to inform estimates of plant productivity in global carbon cycle models  
65 (Campbell et al., 2017a; Hilton et al., 2017; Launois et al., 2015).

66  
67 OCS fluxes have not been previously reported for old-growth forests, although a recent  
68 study using flask samples inferred large uptake of OCS in coastal redwood forests in  
69 northern California (Campbell et al., 2017b). Rastogi et al. (in revision) found large  
70 drawdowns in mixing ratios of OCS at an old growth forest in the Pacific Northwestern  
71 U.S., and significant uptake of this gas by various components of the ecosystem (leaves,  
72 soils, and epiphytes). In this study we report estimates of OCS fluxes from an old-growth  
73 forest and place them in the context of ecosystem carbon and water cycling. Additionally  
74 we investigate the response of CO<sub>2</sub>, H<sub>2</sub>O and OCS fluxes to changes in the fraction of  
75 downwelling diffuse radiation, as well as heat wave events through the growing season.  
76 Technological constraints posed limitations in measuring fast-response OCS fluxes so  
77 instead we combine continuous in-situ measurements of OCS mixing ratios above and  
78 within the canopy with established theoretical equations for OCS uptake (see Berry et al.,  
79 2013; Commane et al., 2015; Seibt et al., 2010) to characterize OCS fluxes using a simple  
80 empirical model and compare them with ecosystem uptake of CO<sub>2</sub> from co-located eddy  
81 covariance measurements.

82

## 83 2. Methods

### 84 2.1. Site Description

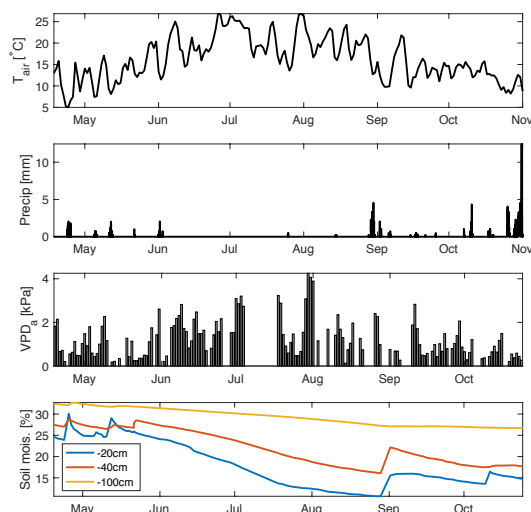
85 Measurements were made at the Wind River Experimental Forest (WR), located within  
86 the Gifford Pinchot National Forest in southwest Washington state, USA (45°49'13.76"  
87 N; 121°57'06.88"; 371 m above sea level). The site is well studied and described in great  
88 detail (Paw U et al., 2004; Shaw et al., 2004; Wharton and Falk, 2016; Winner et al.,



89 2004). The climate is classified as temperate oceanic with a strong summer drought. The  
90 forest is 478 ha of preserved old-growth evergreen needle-leaf forest, with dominant tree  
91 species of Douglas fir (*Pseudotsuga menziesii*) and Western hemlock (*Tsuga*  
92 *heterophylla*). The tallest Douglas fir trees are between 50 and 60m, while the shade-  
93 tolerant hemlocks are typically between 20-30 m high. Maximum rooting depth is 1–2 m  
94 for the tallest, dominant Douglas-fir trees although most of the root biomass is  
95 concentrated in the first 0.5 m (Shaw et al., 2014). The cumulative LAI is estimated to be  
96 8-9 m<sup>2</sup> m<sup>-2</sup> (Parker et al., 2004). Additionally, the ecosystem hosts a large diversity of  
97 mosses, lichens and other epiphytic plants, which play an important role in canopy OCS  
98 dynamics (Rastogi et al., in revision). The soils are volcanic in origin, although most of  
99 the forest surface is comprised of decaying organic matter (Shaw et al., 2004).

100

101 2.2. Study period: Measurements reported here are between April 18- Dec 31, 2015.  
102 However, in early November an intake line at the top of the canopy was damaged after a  
103 rainstorm. Measurements continued at the other intake heights (see sections 2.4 and 2.9).  
104 Therefore ecosystem fluxes and related analyses in this study cover 136 days between  
105 April 18 and October 31, while chamber based soil fluxes are reported for the months of  
106 August-December. Gaps in the time series due to analyzer maintenance correspond to Jun  
107 26-28, July 6-17, August 4-7, August 24 and October 4-7. April-October roughly  
108 corresponds to most of the growing season, although at this site GPP usually peaks early  
109 in March-April, when soil moisture is high and ecosystem respiration flux is low, while  
110 plant productivity is typically severely light and temperature limited in the months of  
111 November-December (Wharton and Falk, 2016). Environmental conditions during the  
112 measurement campaign are shown in Figure 1 are represent a typical Mediterranean-type  
113 climate, with temperature peaking in July and minimal to no measured rainfall between  
114 June and September. This results in high summertime atmospheric vapor pressure deficit  
115 (VPD<sub>a</sub>), and soil moisture declines steadily through the summer period, with some  
116 recharge following rare precipitation events in September and then more commonly in  
117 October. The measurement period also encompasses three distinct heat waves,  
118 characterized by anomalously high air temperatures and mid-day VPD<sub>a</sub> values (often  
119 exceeding 4 kPa). We examine the response of OCS and CO<sub>2</sub> fluxes during these heat  
120 waves.



121

122

123

124

Figure 1. Environmental conditions at Wind River during the measurement campaign. daily mean air temperature (a), precipitation (b) Mid-day VPDa (c) and Soil moisture measured at three depths (d).

125

126

127

128

129

130

131

132

133

134

135

136

137

138

139

140

141

142

143

144

145

146

147

148

149

2.3. CO<sub>2</sub> and H<sub>2</sub>O eddy flux measurements: Carbon, water and energy fluxes have been collected since 1998 at the Wind River AmeriFlux tower (US-wrc; Paw U et al. 2004). For further details readers are referred to Falk et al., (2008; instrumentation and data processing), and Wharton et al., (2012) and Wharton and Falk, (2016) for multi-year carbon and water flux measurements and synthesis.

2.4. OCS measurements: A commercially available off-axis integrated cavity output spectroscopy analyzer manufactured by Los Gatos Research Inc., (LGR; model 914-0028) was deployed at the base of the tower in an insulated and temperature-controlled shed. The instrument measures mixing ratios of OCS, CO<sub>2</sub>, H<sub>2</sub>O and CO simultaneously at a maximal scan rate of 5Hz. The system uses a 4.87 μm cascade laser coupled to a high finesse 800 cm<sup>3</sup> optical cavity and light transmitted through the cavity is focused into a cooled and amplified HgCdTe detector. OCS is detected at ~2050.40 cm<sup>-1</sup>, CO<sub>2</sub> at 2050.56 cm<sup>-1</sup>, CO at ~2050.86 cm<sup>-1</sup>, and H<sub>2</sub>O at ~2050.66 cm<sup>-1</sup>. Pressure broadening associated with changes in the concentration of water vapor in the samples is corrected for in the analysis routine. Air was sampled through 0.25'' diameter PFA tubing using a diaphragm pump at a flow rate of 2L min<sup>-1</sup>, from inlets located at 70m (at the height of the eddy flux instrumentation), 60m (canopy top), 20m, 10m, and 1m. The sampling frequency was 0.1Hz and the sampling interval was 5 minutes. The first minute of each sampling interval was removed to avoid any inter-sampling mixing. The remaining data were checked for temperature and pressure fluctuations inside the measurement chamber, and a moving window filter was used to eliminate any sudden outliers in the data. Mixing ratios were aggregated to provide hourly means. For detailed information regarding instrumentation and the measurement readers are referred to Rastogi et al (in revision), Berkelhammer et al. (2014) and Belviso et al. (2016).



150 2.5. Calibration: Calibration was performed using ambient air stored in insulated tanks as  
 151 a secondary reference. Air was sampled into the analyzer daily, and tank pressure was  
 152 routinely monitored to check for leaks. Glass flasks were randomly sampled from  
 153 calibration tanks and measured against a NOAA GMD reference standard. Cross-  
 154 referencing revealed that the accuracy of the measurement was within the reported  
 155 minimum uncertainty of the instrument (of  $12.6 \text{ pmol mol}^{-1}$ ; Berkelhammer et al., 2016).

156  
 157 2.6. Thermal Camera measurements: Leaf temperatures were measured from October 28,  
 158 2014 to January 28, 2016 using a FLIR A325sc thermal camera (FLIR System Inc.,  
 159 Wilsonville, OR), in which a FLIR IR 30-mm lens (focal length: 30.38 mm; field of  
 160 view:  $15^\circ \times 11.25^\circ$ ) was installed. The thermal camera has a pixel resolution of  $320 \times 240$ .  
 161 Within the field of view (FOV), spot sizes of a single pixel are 0.83 cm from 10-m  
 162 distance and 8.3 cm from 100-m distance. Manufacturer-reported errors in original  
 163 measured thermal temperatures are  $\pm 2^\circ \text{C}$  or  $\pm 2\%$  of the measurements. The camera  
 164 model is identical to one used in another study at an AmeriFlux site in central Oregon  
 165 (US Me-2), and the detailed specifications can be found in Kim et al. (2016). To monitor  
 166 a larger canopy region, a pan-tilt unit (PTU) was used for motion control, allowing  
 167 multiple canopy thermal image acquisition within one motion cycle. We used a FLIR  
 168 PTU-D100E (FLIR System Inc., Wilsonville, OR; (<http://www.flir.com/mcs>)) to move the  
 169 thermal camera vertically and horizontally at specific pan and tilt angles. We selected  
 170 five pan-tilt angle (PT) positions representing the upper canopy (i.e.,  $\sim 40$  to 60 m above  
 171 the forest floor) to estimate leaf temperatures in this study.

172 2.7. Diffuse light measurement and analyses: An SPN1 Sunshine Pyranometer (Delta-T  
 173 Devices Ltd., Cambridge, U.K.) was installed at the top of the canopy and collected direct  
 174 and diffuse shortwave downwelling radiation from April- December 2015. Measurements  
 175 were made every 1 min, and then aggregated to hourly means. We limited our analyses of  
 176 diffuse radiation data to include only mid-day hours (between 11am-1pm) to minimize  
 177 the influence of solar angles on diffuse radiation fractions. We defined three distinct  
 178 periods based on the ratio of diffuse radiation to total incoming solar radiation (*fdiff*).  
 179 Data were characterized as clear if *fdiff* < 0.2; partly cloudy if *fdiff* > 0.2 and *fdiff* < 0.8,  
 180 and overcast if *fdiff* > 0.8.

181 2.8. OCS flux estimation: Canopy OCS flux was estimated using flux-gradient similarity,  
 182 following Commane et al., 2015.

$$183 \quad F_{\text{OCS}} = F_{\text{H}_2\text{O}} \cdot \frac{g_{\text{OCS}}}{g_{\text{H}_2\text{O}}} \quad (1)$$

184  
 185 where  $F_{\text{OCS}}$ ,  $F_{\text{H}_2\text{O}}$ ,  $g_{\text{OCS}}$  and  $g_{\text{H}_2\text{O}}$  are the fluxes and gradients of OCS and  $\text{H}_2\text{O}$ ,  
 186 respectively. Following Seibt et al., (2010) and Berry et al., (2013), we assume that OCS  
 187 is irreversibly and rapidly consumed inside leaves, such that the gradient between  
 188 ambient air and the leaf interior effectively reduces to the ambient measured OCS mixing  
 189 ratio:

$$191 \quad g_{\text{OCS}} = \chi_{\text{OCS}}^a - \chi_{\text{OCS}}^l = \chi_{\text{OCS}}^a, \quad (3)$$

192 where  $g_{\text{OCS}}$  is defined as the gradient of OCS between ambient air and the leaf  
 193 intercellular spaces ( $\chi$  is the mixing ratio of OCS and superscripts *a* and *l* refer to ambient



194 and leaf respectively). In our study,  $\chi_{OCS}^a$  is the measured mixing ratio at the canopy top  
 195 (60m) instead of above canopy (70m) to account for the boundary layer resistance, the  
 196 effect of which is likely low in tall and heterogeneous coniferous forests. We use vapor  
 197 pressure deficit (VPD) as the corresponding gradient for H<sub>2</sub>O, under the key assumption  
 198 that the intercellular leaf surfaces are saturated with water vapor. While VPD is usually  
 199 calculated using air temperature, a more accurate calculation can be performed with leaf  
 200 temperatures, which can deviate significantly from air temperatures (Kim et al. 2016),  
 201 leading to significant differences between the VPD of ambient air and that at the leaf  
 202 surface (Fig. 2a and 3d in this study). Previously leaf temperatures have been inferred  
 203 from sensible heat fluxes, wind speed and air temperatures (e.g. Wehr et al., 2017), here  
 204 we use explicit measurements of leaf skin temperatures to estimate leaf-air VPD (VPD<sub>l</sub>).  
 205 Analogous to Eq (3),  
 206

$$207 \quad g_{H_2O} = \chi_{H_2O}^l - \chi_{H_2O}^a = \frac{(e_s - e_a)}{P} = \frac{VPD_l}{P}, \quad (4)$$

208 where  $e_s$  is saturation vapor pressure at the leaf surface (kPa), using leaf skin temperature,  
 209  $e_a$  is the actual vapor pressure (kPa),  $P$  is the measured atmospheric pressure (Pa) at the  
 210 tower top, and  $\chi_{H_2O}^l$  and  $\chi_{H_2O}^a$  (ppth) are the leaf and ambient H<sub>2</sub>O mixing ratios at the  
 211 canopy top. Finally, since gradients of OCS and H<sub>2</sub>O are estimated between ambient air  
 212 and the leaf intercellular spaces, these are normalized by the ratio of diffusivities of these  
 213 two species in air (Seibt et al., 2010; Wohlfahrt et al., 2012).  
 214

215  $F_{H_2O}$  was measured using eddy covariance at the tower top (70m). In high LAI forests  
 216 with minimal exposed soil, such as those of the Pacific Northwest, fluxes of  $F_{H_2O}$  can be  
 217 treated as a good proxy for transpiration, since soil evaporation should be minimal. We  
 218 excluded rainy days, as well as two days following rainfall, to only capture periods when  
 219  $F_{H_2O}$  can be assumed to be dominated by transpiration. We included nighttime data since  
 220 several temperate tree species are known to transpire during the night (Dawson et al.,  
 221 2007). Moreover, in this particular forest OCS is taken up by epiphytes under conditions  
 222 of high humidity, which are common at nighttime (Rastogi et al., in revision). The first  
 223 term in right hand side of equation (1) was evaluated only under the condition  $F_{H_2O} > 0.2$   
 224  $\text{mmolm}^{-2}\text{s}^{-1}$ . When this condition was not met (e.g. at nighttime), fluxes were calculated  
 225 using by integrating the rate of change in hourly OCS mixing ratios through the entire  
 226 profile.  
 227

228 Leaf Relative uptake was calculated following Seibt et al (2010).  
 229

$$230 \quad LRU = \frac{F_{OCS}}{GPP} \cdot \frac{\chi_{CO_2}}{\chi_{OCS}}, \quad (5)$$

231  
 232 where GPP was estimated from CO<sub>2</sub> fluxes measured at the tower top. Finally, canopy  
 233 conductance ( $G_c$ ) was calculated by inverting the Penman Monteith equation (Monteith,  
 234 1965), which uses a combination of micrometeorological and eddy flux data collected  
 235 above the canopy at the tower top.  $G_c$  is the canopy-scale equivalent of stomatal  
 236 conductance, with the assumption that the canopy (or ecosystem) acts as a single big leaf.



237

$$G_c = \left[ \frac{\rho C_p \delta e}{\gamma L_e} + \frac{\left(\frac{\Delta}{\gamma}\right)^{\beta-1}}{G_a} \right]^{-1}, \quad (6)$$

238

239

240

241

242

243

244

245

246

247

248

249

250

251

252

253

254

255

256

257

258

259

where  $\rho$  is air density ( $\text{kg m}^{-3}$ ),  $C_p$  is specific heat ( $\text{J kg}^{-1}\text{K}^{-1}$ ),  $\delta e$  is vapor pressure deficit (kPa),  $\gamma$  is the psychrometric constant ( $\text{kPa K}^{-1}$ ),  $\Delta$  is the slope of the saturation vapor pressure curve ( $\text{kPa K}^{-1}$ ),  $\beta$  is the Bowen ratio (H:LE), and  $G_a$  is the aerodynamic conductance for momentum transfer, calculated as  $u^{*2} \cdot u^{-1}$  (where  $u^*$  is the friction velocity calculated from the momentum fluxes and  $u$  is the horizontal wind speed).  $G_a$  provides a measure of how well the canopy top is coupled to the background atmosphere (Wharton et al., 2012).

2.9. Surface Fluxes: A long-term automatic soil survey chamber (Li-Cor 8100-104, 20 cm diameter) was installed at three  $0.03 \text{ m}^2$  surface sites in series, within 1 meter of each other. All plastic and rubber parts had been removed from the chamber and replaced with materials compatible with OCS measurements: stainless steel, PFA plastic, and Volara foam. Blank measurements were performed in the laboratory before deployment and OCS concentrations in the chamber were found to be indistinguishable from incoming ambient concentrations. The stainless steel chamber top opened and closed automatically on a timer. Gas was drawn through the chamber via a pump downstream of the analyzer, and the  $3 \text{ Lmin}^{-1}$  flow rate was confirmed with a mass flow meter. When the chamber was open, ambient near-surface air was observed. When the chamber was closed, trace gas concentrations reached a stable state for at least 2 minutes during the 10-minute incubation time. The difference between the ambient concentration and the stable closed-chamber concentration were used to calculate the surface fluxes of OCS and  $\text{CO}_2$ .

260

261

262

263

264

265

266

267

268

269

270

271

272

273

274

275

276

277

278

$$F_{forest\ floor} = M_c \Delta \chi \cdot A^{-1}, \quad (7)$$

where  $M_c$  is the measured flow rate into the chamber (converted from  $\text{Lmin}^{-1}$  to  $\text{mols}^{-1}$  using the ideal gas law) and  $\Delta \chi$  is the difference between mixing ratios of OCS or  $\text{CO}_2$  in ambient air and the chamber and  $A$  is the surface area of the chamber. The minimum flux detectable with this method was  $1.2 \text{ pmolm}^{-2}\text{s}^{-1}$  uptake or production.

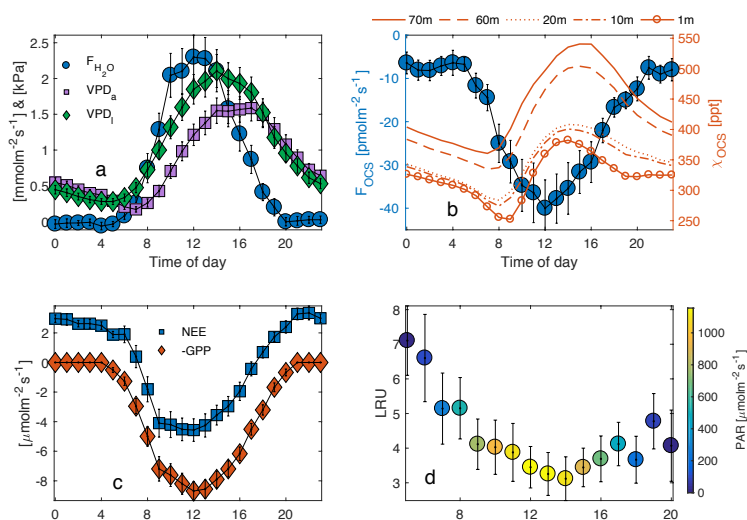
Care was taken to select sites characteristic of the surface, which was generally springy and covered in a mat of mosses and lichen. Surface flux observations were made at site 1 from July 6 to 16, site 2 from August 13 to October 7, and site 3 from November 6 to December 2, 2015. The first site was visually similar to the subsequent two sites at the surface, though the chamber base of the first site was installed into the moss layer and a barely decomposed fallen tree. When a soil sample was attempted to be extracted from the footprint of the chamber base, several liters of in tact wood litter were removed. The influence of the developed soil on site 1 is therefore considered minimal. Site 2 was selected nearby and observations were made until a dominant tree fell on the soil chamber. The chamber was repaired and re-installed a month later at site 3 and observations continued without incident until the chamber was removed in advance of the soil freezing.

### 276 3. Results and Discussion:

277 3.1. Ecosystem fluxes: The composite diurnal cycles for  $\text{CO}_2$ , water vapor and OCS and  
 278 fluxes are shown (Fig. 2a-c). The total ecosystem flux of OCS ( $F_{\text{OCS}}$ ; Fig 2.b.) follows a



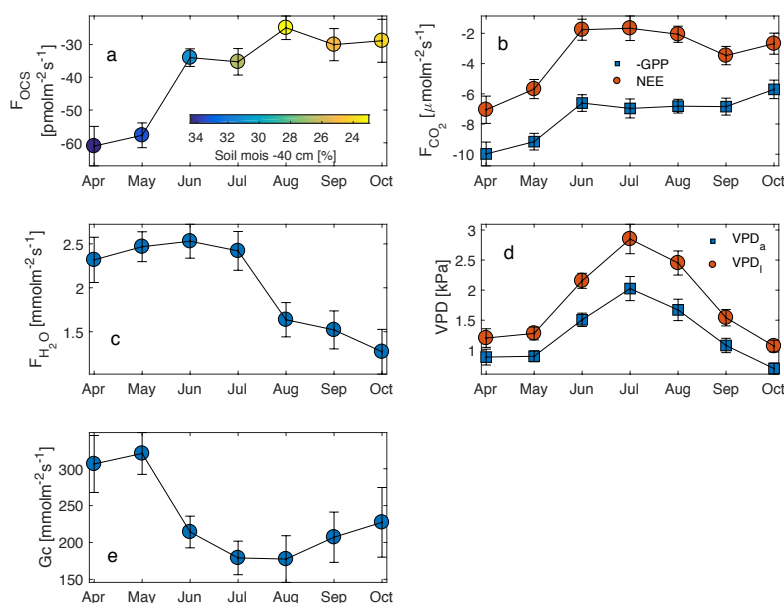
279 pronounced diurnal cycle that peaks during daylight hours. The vertical profile of mixing  
280 ratios measured throughout the canopy is also shown (right y-axis and orange lines in  
281 Fig.2.b). OCS mixing ratios are highest at the canopy top and lowest near the forest floor,  
282 but mixing ratios increase from the early morning to mid-afternoon. Together these  
283 processes are indicative of ecosystem uptake and downward entrainment of boundary  
284 layer air. While entrainment helps explain the diurnal cycle of observed mixing ratios,  
285 this flux integrates to zero at daily and longer time scales (Rastogi et al., in revision). The  
286 shape of the  $F_{\text{OCS}}$  curve is very similar to those of net and gross carbon fluxes (Fig 2.b),  
287 although  $F_{\text{OCS}}$  was consistently negative throughout the 24-hour period, implying  
288 ecosystem uptake during nighttime and daylight hours. While nighttime uptake of OCS  
289 (mean nighttime flux  $\sim -10 \pm 1 \text{ pmolm}^{-2}\text{s}^{-1}$ ) is likely due to a combination of soil,  
290 epiphyte, and vascular plant uptake due from partially closed stomata, daytime uptake is  
291 likely dominated by vascular plant stomatal activity. Leaf relative uptake, a ratio of  
292  $F_{\text{OCS}}:\text{GPP}$  normalized by the mean mixing ratios of  $\text{OCS}:\text{CO}_2$ , showed a strong light  
293 dependence. High-light, mid-day values ranged between 3-4, which is higher than those  
294 observed at other forest systems (Kooijmans et al., 2017; Wehr et al., 2017) but well  
295 within the spread of values obtained in a recent meta-analyses of OCS studies for  
296 vegetated ecosystems (Whelan et al., 2018). The diurnal cycle was found to be  
297 asymmetric, with peak values observed in the early morning, when stomatal conductance  
298 is likely to be high (Winner et al., 2004), but GPP is limited by low light levels. It is  
299 important to note that LRU is likely influenced by large amounts of epiphyte and  
300 understory vegetation, which assimilate OCS even at times when ecosystem  $\text{CO}_2$  uptake  
301 is low or zero. Epiphytic assimilation of OCS is highly influenced by moisture content  
302 (Gimeno et al., 2017) and is typically higher through the night and in the early mornings  
303 at this site (Rastogi et al., in revision). Moreover, in tall old-growth forests, leaf area is  
304 vertically distributed over a much larger part of the canopy compared to other forests  
305 (Parker et al., 2004). While leaves at the canopy top exercise tight stomatal control to  
306 limit water loss and minimize hydraulic failure (Woodruff et al., 2007) leaves lower  
307 down in the canopy, including those of understory vegetation, likely impose less stomatal  
308 control of transpiration (Winner et al., 2004). Lower-canopy leaves may therefore  
309 continue to disproportionately assimilate OCS, even under low rates of carbon  
310 assimilation (as  $\text{CO}_2$  uptake is additionally light limited).



311

312 Figure 2. Diurnal cycle of H<sub>2</sub>O flux (blue circles) and VPD estimated from air and leaf  
 313 temperatures (purple squares and green diamonds respectively; a), estimated OCS flux  
 314 (circles, left axis) and mixing ratio profile (right axis; b), NEE and GPP (blue squares and  
 315 red diamonds; c), and leaf relative uptake (calculated only during daylight hours, colors  
 316 represent Photosynthetically active radiation; d).

317 3.2. Seasonal dynamics: Daytime fluxes of OCS and CO<sub>2</sub> followed similar patterns (Fig.  
 318 3a-b). Ecosystem uptake of OCS and CO<sub>2</sub> (as well as GPP) was highest in April, and  
 319 declined as the soil drought progressed. Mean monthly maximum OCS flux was  
 320 estimated as  $-61 \pm 6 \text{ pmolm}^{-2}\text{s}^{-1}$ , while daily mean maximum GPP over this period was  
 321 estimated as  $10 \pm 1 \mu\text{molm}^{-2}\text{s}^{-1}$  (plotted as a negative quantity in Fig. 3b to show  
 322 ecosystem uptake). While the steepest declines in F<sub>OCS</sub>, NEE and GPP happened between  
 323 the months of May and June, F<sub>OCS</sub> continued to decline through the rest of the summer,  
 324 with a minimum in August, incrementally increasing in September and decreasing again  
 325 in October. CO<sub>2</sub> fluxes flattened between June-September, before declining again in  
 326 October. During mid-late summer, water vapor flux declined (Fig.3c), as plants exercised  
 327 greater control over stomata responding to high VPD (peaking in July; Fig 3d). This can  
 328 be clearly seen in the seasonal cycle of canopy conductance (G<sub>c</sub>; Fig. 3e) calculated  
 329 using the Penman-Monteith method. Mean monthly G<sub>c</sub> was highest in the months of  
 330 April and May, and then declined precipitously with soil moisture, before increasing  
 331 again slightly in September and October following soil recharge and decreased VPD due  
 332 to precipitation events. At the monthly scale, patterns of daytime F<sub>OCS</sub> were most similar  
 333 to those of G<sub>c</sub> and followed trends in soil moisture. In October, soil water recharge,  
 334 several rain-free days, and lower VPD (Fig. 1) do not result in increased gas exchange,  
 335 likely due to downregulation of photosynthesis (Eastman and Camm, 1995), induced by  
 336 photoprotective changes in the xanthophyll cycle (Adams and Demmig-Adams, 1994).



337

338 Figure 3. Monthly means for daytime  $F_{OCS}$  colored according to soil moisture at 40cm  
 339 depth, NEE and -GPP (red circles and blue squares; b), water vapor flux (c),  $VPD_a$  and  
 340  $VPD_l$  (blue squares and red circles; d), and canopy conductance ( $G_c$ ; e).

341 3.3. Nighttime ecosystem and Surface Fluxes: While daytime fluxes of OCS and  $CO_2$   
 342 were indicative of seasonal changes in ecosystem productivity and conductance,  $F_{OCS}$  and  
 343  $F_{CO_2}$  were driven by different environmental conditions during the night. Ecosystem  
 344 respiration is modeled based on temperature and therefore peaked in July (when air  
 345 temperature was highest). Nighttime  $F_{OCS}$  however, was more related to soil moisture  
 346 status (blue circles in Fig. 4a-b). Nighttime  $F_{OCS}$  was highest in April (mean =  $-12.7 \pm 2.6$   
 347  $\text{pmol m}^{-2} \text{s}^{-1}$ ), lowest between June and August (mean =  $-5.9 \pm 1.5 \text{ pmol m}^{-2} \text{s}^{-1}$ ) and  
 348 increased again in October (mean =  $-9.7 \pm 2.2 \text{ pmol m}^{-2} \text{s}^{-1}$ ). Nighttime uptake of OCS at  
 349 the site is likely due to soil (see below), epiphytes (Rastogi et al., in revision; Gimeno et  
 350 al., 2017), and incomplete stomatal closure (Kooijmans et al., 2017).

351 Forest floor OCS fluxes were observed from 3 sites in series and within 1 m of each  
 352 other. Site 1 had approximately twice the OCS uptake compared to the subsequent two  
 353 sites and had a substantial layer of intact woody debris under the chamber footprint. Site  
 354 2 and 3 had OCS fluxes similar to previous surface fluxes reported for forests (Whelan et  
 355 al., 2018). For all sites, there was no clear diurnal pattern. For site 2, uptake immediately  
 356 following chamber installation was higher ( $\sim 6 \text{ pmol m}^{-2} \text{s}^{-1}$ ) than fluxes later on (all  $< 6$   
 357  $\text{pmol m}^{-2} \text{s}^{-1}$ ) when temperatures were lower. Site 3 did not have high uptake after  
 358 chamber installation, and had consistent fluxes between the detection limit and  $-6.2 \text{ pmol}$   
 359  $\text{m}^{-2} \text{s}^{-1}$  for the first few weeks. When ambient air temperatures dropped below freezing,  
 360 uptake remained unchanged, except for the largest uptake observed (6 to  $12 \text{ pmol m}^{-2} \text{s}^{-1}$ )  
 361 during two events when average air temperature fluctuated from a cooling to warming  
 362 trend. Soil temperature never dropped below freezing during the experiment and was

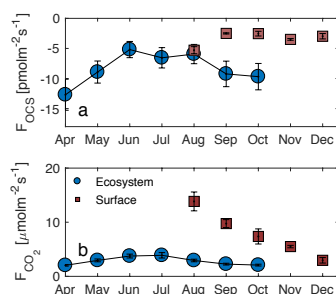


363 generally colder over time. We did not observe any OCS emissions from the chamber  
 364 based measurements, consistent with recent studies that find that cooler, moist (Maseyk  
 365 et al., 2014; Sun et al., 2016; Whelan et al., 2016) and radiation limited (Kitz et al., 2017)  
 366 soils do not emit OCS.

367 Surface CO<sub>2</sub> emissions exhibited a relationship with temperature, where highest  
 368 production (~25 μmol m<sup>-2</sup>s<sup>-1</sup>) corresponded with temperatures ~15°C, and maximum flux  
 369 values decreased for warmer and colder temperatures. CO<sub>2</sub> emissions had a diurnal  
 370 pattern, with lowest emissions at night and maximum emissions in late morning to mid  
 371 afternoon. No obvious relationship emerges from CO<sub>2</sub> emission and OCS uptake, though  
 372 the high OCS uptake events in late November and early December have a linear  
 373 relationship with CO<sub>2</sub> emissions. For sites 2 and 3, the ratio of OCS emission to CO<sub>2</sub>  
 374 production, normalized by the concentration of OCS and CO<sub>2</sub> in the closed chamber, was  
 375 between -0.25 and -3.5 with a mean of -1. In contrast, the same ratio for site 1 varied  
 376 from -5 to -19 with a mean of -10.

377 At the peak of the soil drought (August; Fig. 1d), nighttime ecosystem OCS flux was  
 378 similar to the chamber-based surface fluxes, after which magnitudes differed by a factor  
 379 of 2-3. This difference can be explained by epiphytic consumption of OCS. Epiphytes are  
 380 a moisture dependent sink OCS at the site (Rastogi et al., in revision) and therefore are  
 381 likely inactive during the warmest and driest part of the year. Surface fluxes of CO<sub>2</sub> on  
 382 the other hand were much higher than ER estimated from the flux tower (blue circles in  
 383 Fig. 4b). While there are issues in scaling up chamber-based estimates, these results  
 384 corroborate earlier work that suggest that flux tower based estimates of ER at this site  
 385 might be underestimated (Harmon et al., 2004).

386



387

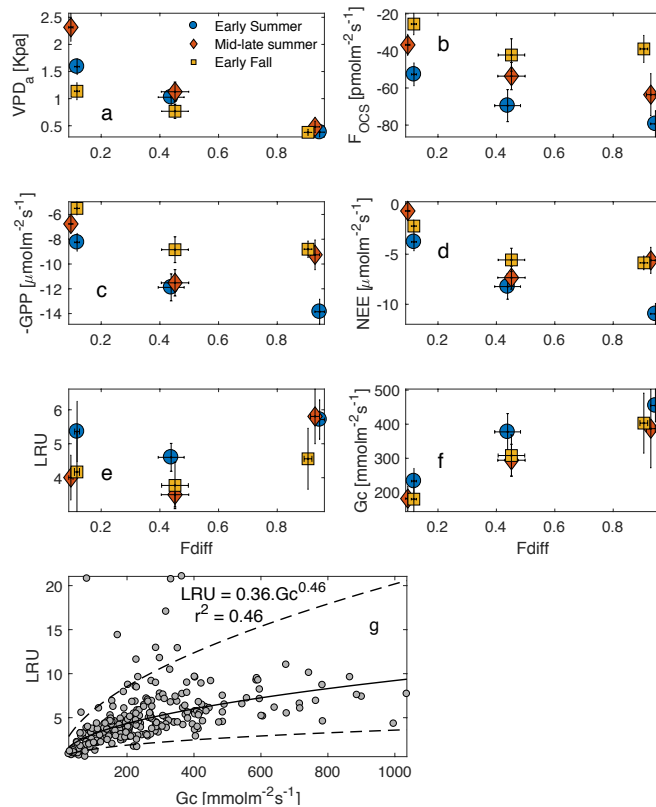
388 Figure 4. Nighttime ecosystem F<sub>OCS</sub> and F<sub>CO<sub>2</sub></sub> (blue circles in a-b) and Surface F<sub>OCS</sub> and  
 389 F<sub>CO<sub>2</sub></sub> from chamber measurements (brown squares in a-b) from sites 2 and 3. Site 1 was  
 390 atypical (see section 2.7) and therefore fluxes are not shown. Values for site 1 F<sub>OCS</sub> and  
 391 F<sub>CO<sub>2</sub></sub> were -22 ± 0.3 pmol m<sup>-2</sup> s<sup>-1</sup> and -83 ± 2 μmol m<sup>-2</sup> s<sup>-1</sup> respectively.

392 3.4. Sensitivity to diffuse light: Mid-day fluxes of OCS and CO<sub>2</sub> were found to be  
 393 sensitive to changes in the fraction of diffused:total incoming shortwave radiation (*f<sub>diff</sub>*;  
 394 Figure 5a-b). For these analyses, data were separated into three periods corresponding to  
 395 early summer (DOY 109-180), mid-late summer (DOY 180-240) and early fall (DOY  
 396 240-297), and binned into three categories: clear sky conditions, partly cloudy, and  
 397 overcast, defined in sec. 2.7. Mid-day VPD was highest under clear sky conditions and  
 398 lowest under overcast skies, but was most different across the three periods, during clear  
 399 skies (Fig. 5a). Consequently, OCS and CO<sub>2</sub> uptake was highest (most negative fluxes)



400 under overcast conditions during the early summer, and generally declined as  $f_{diff}$   
401 decreased across all time periods (Fig. 5b-d). Across the three periods, the rate of  
402 decrease was much higher as  $f_{diff}$  changed from partially cloudy to clear. During the mid-  
403 late summer, however, (red diamonds in Fig. 5a-f), the diffuse light effect resulted in  
404 GPP and NEE being almost as high as during the early summer.  $F_{OCS}$  was also highest  
405 under partially cloudy skies during this time, and only showed a very weak decline under  
406 completely overcast conditions. Overall, the behavior of OCS and  $CO_2$  fluxes was similar  
407 during the later time periods. Leaf relative uptake (LRU; calculated according to eq. 5)  
408 was lowest under partly clear skies and highest under overcast conditions. This is because  
409 under highly diffuse conditions, carbon uptake is additionally limited by light, whereas  
410  $F_{OCS}$  is not (Wehr et al., 2017; Maseyk et al., 2014). The shape of the LRU curves can  
411 additionally be explained by examining canopy conductance ( $G_c$ ; Fig. 5f), which was  
412 also higher under overcast skies. LRU increased with  $G_c$  across all three periods (Fig.  
413 5g), and appeared to be constant for  $G_c$  greater than  $\sim 400 \text{ mmol m}^{-2} \text{ s}^{-1}$ .

414 The diffuse light enhancement of stomatal and canopy conductance is well documented  
415 across a range of forest ecosystems (Alton et al., 2007; Cheng et al., 2015; Hollinger et  
416 al., 2017; Urban et al., 2007; Wharton et al., 2012). Lower VPD (Fig. 5a) and light levels  
417 allow plants to keep stomata open at mid-day and continue fixing  $CO_2$ . Lower VPD  
418 reduces transpirational losses, and the lack of VPD-induced partial stomatal closure  
419 reduces the resistance to  $CO_2$  diffusion into the leaf. Correspondingly, the less directional  
420 nature of diffuse solar radiation allows greater penetration into the canopy, thus  
421 increasing photosynthesis across the entire canopy, even as a reduction in canopy top leaf  
422 photosynthesis is observed due to a reduction in total radiation. In a multi-year analysis at  
423 Wind River, Wharton et al., (2012) found that cloudy and partly cloudy sky conditions  
424 during the peak-growing season lead to an enhancement of NEE. During our study,  $G_c$   
425 was generally higher in the early growing season, but increased as sky conditions  
426 changed from clear skies to overcast. This increase was similar across the three time  
427 periods, even as the response of OCS and  $CO_2$  fluxes was different across these periods.  
428 This indicates that declining soil moisture (Fig. 1d) likely limits gas exchange as the  
429 summer progresses, even as canopy conductance can be reasonably high under overcast  
430 skies.



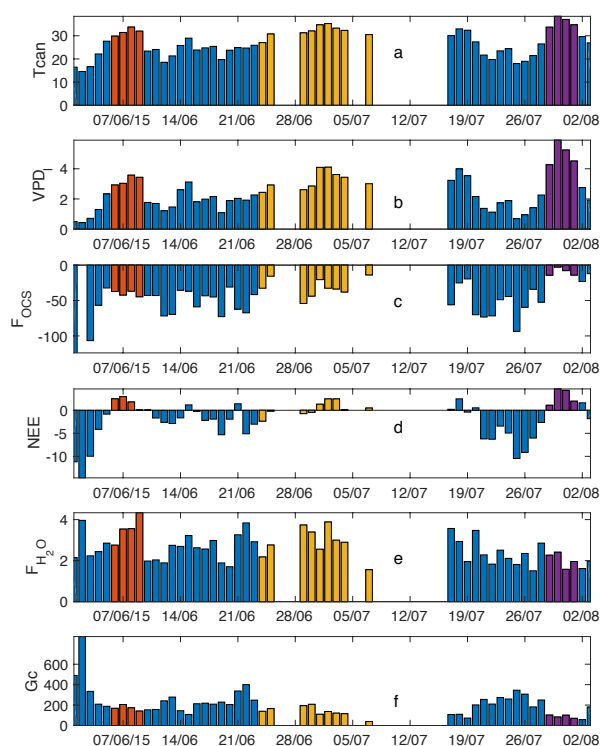
431

432 Figure 5. Mid-day VPD<sub>a</sub>, F<sub>ocs</sub>, NEE and GPP plotted against the fraction of diffuse  
 433 downwelling shortwave radiation (a-d) for early summer, mid-late summer and early fall  
 434 of 2015 (these periods are defined in Section 3.4). High values on the x-axis indicate  
 435 completely overcast or cloudy conditions, whereas as low values indicated clear skies.  
 436 LRU increases with increasing *f<sub>diff</sub>* during each period but the increase is most  
 437 pronounced in the early summer (e). G<sub>c</sub> increases from clear to partly cloudy conditions  
 438 across the three periods and plateaus during overcast sky conditions (f). Across the three  
 439 periods, LRU increased with G<sub>c</sub>, and levelled off at G<sub>c</sub> values greater than ~ 400  
 440 mmolm<sup>-2</sup>s<sup>-1</sup> (g).

441 3.5. Response to heat waves: 2015 was the warmest year in large parts of the Pacific  
 442 Northwest since records began in the 1930s (Dalton et al., 2017). We observed three  
 443 distinct heat waves during the 2015 summer. These were in early June (DOY 157-160),  
 444 end of June- early July (DOY 175-188) and late July-early August (DOY 210-213). The  
 445 three heat waves are shown as red, yellow and dark purple lines in Fig. 5; the overall time  
 446 series is shown in blue (mid-day means are plotted for all variables). Mid-day  
 447 temperatures exceeded 30°C during these heat wave events, while VPD-leaf exceeded  
 448 3Kpa during the first heat wave and increased to a maximum of 5.3 kPa during the last  
 449 event (Fig. 5b). During the first two events, F<sub>ocs</sub> was similar to days immediately prior  
 450 (Fig. 5c), but the canopy became a net source of CO<sub>2</sub> during all three events (Fig. 5d).



451 The third events lead to a severe reduction in  $F_{OCS}$ , even though the canopy had received  
452 some rainfall in the preceding weeks (Fig. 1c). Water vapor fluxes (Fig 5e) increased  
453 during the first two heat waves, compared to days immediately prior. The increased water  
454 vapor is likely not from increased transpiration, as canopy scale stomatal conductance  
455 during these events (Gc; Fig. 5f) is dramatically reduced. The increase is rather due to a  
456 flux of water from the soil surface and epiphytes that can store water in the canopy. High  
457 temperatures during such events are likely to result in increased evaporation.



458

459 Figure 6. Mid-day means (11am-1pm local time) for three heat wave periods (plotted as  
460 red, yellow and purple, while the overall time series is shown in blue). Variables  
461 displayed are canopy temperature ( $^{\circ}\text{C}$ ; a), VPD-leaf (b),  $F_{OCS}$  (c), NEE (d), water vapor  
462 flux (e), and canopy conductance (Gc, f). Units for each panel are the same as specified  
463 in previous figures.

#### 464 4. Conclusions

465 Over hourly and seasonal timescales, estimates of  $F_{OCS}$  generally tracked fluctuations in  
466 GPP, implying stomatal control of carbon, water, and OCS fluxes at the site. We used  
467 continuous in-situ measurements of OCS mixing ratios, collocated measurements of  
468 water vapor fluxes, and air and canopy temperatures to calculate OCS uptake. We found  
469 the forest to be a large sink for OCS, with sink strength peaking during daylight hours.  
470 The mean LRU was  $\sim 4$ , and varied in response to changing light conditions and canopy



471 conductance. These LRUs are larger than observed from other ecosystem scale studies,  
472 but well within the range of reported values (Whelan et al., 2018; Sandoval-Soto et al.,  
473 2005). The forest surface was found to be a soil moisture dependent sink of OCS, with  
474 magnitudes that were roughly half of nighttime ecosystem fluxes, indicating other  
475 components of the ecosystem (epiphytes present throughout the canopy and impartial  
476 stomatal closure) to also take up OCS during these hours. Ecosystem fluxes of OCS and  
477 CO<sub>2</sub> were found to be strongly sensitive to the ratio of diffuse:direct radiation reaching  
478 the top of the canopy. Uptake of both OCS and CO<sub>2</sub> increased as sky conditions changed  
479 from clear to partly cloudy. A much smaller increase in uptake was observed as sky  
480 conditions changed from partly cloudy to overcast, except during the early summer, when  
481 soil moisture was not limiting. This change was mediated by the sensitivity of stomata to  
482 changing cloudiness and soil moisture, as estimated from canopy conductance calculated  
483 according to the inverted Penman-Monteith equation. Finally we examined the response  
484 of OCS, CO<sub>2</sub> and H<sub>2</sub>O fluxes on heatwaves, and found that sequential heatwaves lead to  
485 suppression in stomatal gas exchange of all three fluxes.

486 Our results support the growing body of work that suggests ecosystem-scale OCS uptake  
487 is controlled by stomatal dynamics. While moist old-growth forests in Pacific  
488 Northwestern U.S. do not represent a very large fraction of the global terrestrial surface  
489 area, results from this study are likely relevant for other old-growth forests, particularly  
490 high LAI and very wet forests with extensive epiphyte cover, which are widespread in the  
491 humid tropics.

#### 492 Acknowledgements:

493 This work was partly funded by NASA SBIR Phase II award NNX12CD21P to LGR,  
494 Inc. (“Ultrasensitive Analyzer for Realtime, In-Situ Airborne and Terrestrial  
495 Measurements of OCS, CO<sub>2</sub>, and CO.”). We would like to thank the US Forest Service  
496 and the University of Washington for letting us use the research facility at Wind River. In  
497 particular, we wish to sincerely acknowledge Ken Bible and Matt Schroeder for their help  
498 with setting up the experiment as well as maintenance throughout the measurement  
499 campaign. Data collected and used in this study can be accessed at  
500 [ftp.fsl.orst.edu/rastogib/Biogeosciences2018\\_Rastogi](ftp.fsl.orst.edu/rastogib/Biogeosciences2018_Rastogi).

#### 501 References:

502 Adams, W. W. and Demmig-Adams, B.: Carotenoid composition and down regulation of  
503 photosystem II in three conifer species during the winter, *Physiol. Plant.*, 92(3), 451–458,  
504 doi:10.1111/j.1399-3054.1994.tb08835.x, 1994.

505 Alton, P. B., North, P. R. and Los, S. O.: The impact of diffuse sunlight on canopy light-  
506 use efficiency, gross photosynthetic product and net ecosystem exchange in three forest  
507 biomes, *Glob. Chang. Biol.*, 13(4), 776–787, doi:10.1111/j.1365-2486.2007.01316.x,  
508 2007.

509 Asaf, D., Rotenberg, E., Tatarinov, F., Dicken, U., Montzka, S. A. and Yakir, D.:  
510 Ecosystem photosynthesis inferred from measurements of carbonyl sulphide flux, *Nat.*



- 511 Geosci., 6(3), 186–190, doi:10.1038/ngeo1730, 2013.
- 512 Belviso, S., Reiter, I. M., Loubet, B., Gros, V., Lathièrè, J., Montagne, D., Delmotte, M.,  
513 Ramonet, M., Kalogridis, C., Lebegue, B., Bonnaire, N., Kazan, V., Gauquelin, T.,  
514 Fernandez, C. and Genty, B.: A top-down approach of surface carbonyl sulfide exchange  
515 by a Mediterranean oak forest ecosystem in Southern France, *Atmos. Chem. Phys.*  
516 *Discuss.*, (June 2012), 1–25, doi:10.5194/acp-2016-525, 2016.
- 517 Berkelhammer, M., Asaf, D., Still, C., Montzka, S., Noone, D., Gupta, M., Provencal, R.,  
518 Chen, H. and Yakir, D.: Constraining surface carbon fluxes using in situ measurements of  
519 carbonyl sulfide and carbon dioxide, *Global Biogeochem. Cycles*, 28(2), 161–179,  
520 doi:10.1002/2013GB004644, 2014.
- 521 Berkelhammer, M., Steen-Larsen, H. C., Cosgrove, A., Peters, A. J., Johnson, R.,  
522 Hayden, M. and Montzka, S. A.: Radiation and atmospheric circulation controls on  
523 carbonyl sulfide concentrations in the marine boundary layer, *J. Geophys. Res.*, 121(21),  
524 13,113–13,128, doi:10.1002/2016JD025437, 2016.
- 525 Berry, J., Wolf, A., Campbell, J. E., Baker, I., Blake, N., Blake, D., Denning, A. S.,  
526 Kawa, S. R., Montzka, S. A., Seibt, U., Stimler, K., Yakir, D. and Zhu, Z.: A coupled  
527 model of the global cycles of carbonyl sulfide and CO<sub>2</sub>: A possible new window on the  
528 carbon cycle, *J. Geophys. Res. Biogeosciences*, 118(2), 842–852,  
529 doi:10.1002/jgrg.20068, 2013.
- 530 Billesbach, D. P., Berry, J. A., Seibt, U., Maseyk, K., Torn, M. S., Fischer, M. L., Abu-  
531 Naser, M. and Campbell, J. E.: Growing season eddy covariance measurements of  
532 carbonyl sulfide and CO<sub>2</sub> fluxes: COS and CO<sub>2</sub> relationships in Southern Great Plains  
533 winter wheat, *Agric. For. Meteorol.*, 184, 48–55, doi:10.1016/j.agrformet.2013.06.007,  
534 2014.
- 535 Blonquist, J. M., Montzka, S. A., Munger, J. W., Yakir, D., Desai, A. R., Dragoni, D.,  
536 Griffis, T. J., Monson, R. K., Scott, R. L. and Bowling, D. R.: The potential of carbonyl  
537 sulfide as a proxy for gross primary production at flux tower sites, *J. Geophys. Res.*  
538 *Biogeosciences*, 116(4), 1–18, doi:10.1029/2011JG001723, 2011.
- 539 Campbell, J., Berry, J., Seibt, U., Smith, S., Nature, S. M.- and 2017, U.: Large historical  
540 growth in global terrestrial gross primary production, *nature.com*, 544(7468), 84 [online]  
541 Available from: <https://www.nature.com/articles/nature22030> (Accessed 29 January  
542 2018a), 2017.
- 543 Campbell, J. E., Whelan, M. E., Berry, J. A., Hilton, T. W., Zumkehr, A., Stinecipher, J.,  
544 Lu, Y., Kornfeld, A., Seibt, U., Dawson, T. E., Montzka, S. A., Baker, I. T., Kulkarni, S.,  
545 Wang, Y., Herndon, S. C., Zahniser, M. S., Commane, R. and Loik, M. E.: Plant Uptake  
546 of Atmospheric Carbonyl Sulfide in Coast Redwood Forests, *J. Geophys. Res.*  
547 *Biogeosciences*, 122(12), 3391–3404, doi:10.1002/2016JG003703, 2017b.
- 548 Cheng, S. J., Bohrer, G., Steiner, A. L., Hollinger, D. Y., Suyker, A., Phillips, R. P. and  
549 Nadelhoffer, K. J.: Variations in the influence of diffuse light on gross primary



- 550 productivity in temperate ecosystems, *Agric. For. Meteorol.*, 201, 98–110,  
551 doi:10.1016/j.agrformet.2014.11.002, 2015.
- 552 Commane, R., Meredith, L. K., Baker, I. T., Berry, J. A., Munger, J. W., Montzka, S. A.,  
553 Templer, P. H., Juice, S. M., Zahniser, M. S. and Wofsy, S. C.: Seasonal fluxes of  
554 carbonyl sulfide in a midlatitude forest, *Proc. Natl. Acad. Sci.*, 112(46), 14162–14167,  
555 doi:10.1073/pnas.1504131112, 2015.
- 556 Dalton, M. M., Dello, K. D., Hawkins, L., Mote, P. W. and Rupp, D. E.: The third  
557 Oregon climate assessment report, Oregon Clim. Chang. Res. Institute, Coll. Earth,  
558 Ocean Atmos. Sci. Oregon State Univ. Corvallis, OR, 2017.
- 559 Dawson, T., Burgess, S., Tu, K., ... R. O.-T. and 2007, U.: Nighttime transpiration in  
560 woody plants from contrasting ecosystems., *Tree Physiol.*, 27, 561–575, 2007.
- 561 Eastman, P. A. K. and Camm, E. L.: Regulation of photosynthesis in interior spruce  
562 during water stress: changes in gas exchange and chlorophyll fluorescence, *Tree Physiol.*,  
563 15(4), 229–235 [online] Available from: <http://dx.doi.org/10.1093/treephys/15.4.229>,  
564 1995.
- 565 Falk, M., Wharton, S., Schroeder, M., Ustin, S. L. and Paw U, K. T.: Flux partitioning in  
566 an old-growth forest: seasonal and interannual dynamics, *Tree Physiol.*, 28(4), 509–520,  
567 doi:10.1093/treephys/28.4.509, 2008.
- 568 Gimeno, T. E., Ogée, J., Royles, J., Gibon, Y., West, J. B., Burrell, R., Jones, S. P.,  
569 Sauze, J., Wohl, S., Benard, C., Genty, B. and Wingate, L.: Bryophyte gas-exchange  
570 dynamics along varying hydration status reveal a significant carbonyl sulphide (COS)  
571 sink in the dark and COS source in the light, *New Phytol.*, 215(3), 965–976,  
572 doi:10.1111/nph.14584, 2017.
- 573 Harmon, M., Bible, K., Ryan, M., Shaw, D., Chen, H., Klopatek, J. and Li, X.:  
574 Production, Respiration, and Overall Carbon Balance in an Old-growth Pseudotsuga-  
575 Tsuga Forest Ecosystem, *Ecosystems*, 498–512, doi:10.1007/s10021-004-0140-9, 2004.
- 576 Hilton, T., Whelan, M., Zumkehr, A., ... S. K.-N. C. and 2017, U.: Peak growing season  
577 gross uptake of carbon in North America is largest in the Midwest USA, *nature.com*,  
578 7(6), 450 [online] Available from: <https://www.nature.com/articles/nclimate3272>  
579 (Accessed 29 January 2018), 2017.
- 580 Hollinger, A. D. Y., Kelliher, F. M., Byers, J. N., Hunt, J. E., Mcseveny, T. M., Weir, L.,  
581 Ecology, S. and Jan, N.: Carbon Dioxide Exchange between an Undisturbed Old-Growth  
582 Temperate Forest and the Atmosphere Published by : Wiley Stable URL :  
583 <http://www.jstor.org/stable/1939390> REFERENCES Linked references are available on  
584 JSTOR for this article : You may need to log , , 75(1), 134–150, 2017.
- 585 Johnson, J. E., Bandy, A. R., Thornton, D. C. and Bates, T. S.: Measurements of  
586 atmospheric carbonyl sulfide during the NASA Chemical Instrumentation Test and  
587 Evaluation project: Implications for the global COS budget, *J. Geophys. Res.*, 98(D12),



- 588 23443, doi:10.1029/92JD01911, 1993.
- 589 Kim, Y., Still, C. J., Hanson, C. V., Kwon, H., Greer, B. T. and Law, B. E.: Canopy skin  
590 temperature variations in relation to climate, soil temperature, and carbon flux at a  
591 ponderosa pine forest in central Oregon, *Agric. For. Meteorol.*, 226–227, 161–173,  
592 doi:10.1016/j.agrformet.2016.06.001, 2016.
- 593 Kitz, F., Gerdel, K., Hammerle, A., Laterza, T., Spielmann, F. M. and Wohlfahrt, G.: In  
594 situ soil COS exchange of a temperate mountain grassland under simulated drought,  
595 *Oecologia*, 183(3), 851–860, doi:10.1007/s00442-016-3805-0, 2017.
- 596 Kooijmans, L. M. J. J., Maseyk, K., Seibt, U., Sun, W., Vesala, T., Mammarella, I.,  
597 Kolari, P., Aalto, J., Franchin, A., Vecchi, R., Valli, G. and Chen, H.: Canopy uptake  
598 dominates nighttime carbonyl sulfide fluxes in a boreal forest, *Atmos. Chem. Phys.*,  
599 17(18), 11453–11465, doi:10.5194/acp-17-11453-2017, 2017.
- 600 Launois, T., Peylin, P., Belviso, S. and Poulter, B.: A new model of the global  
601 biogeochemical cycle of carbonyl sulfide - Part 2: Use of carbonyl sulfide to constrain  
602 gross primary productivity in current vegetation models, *Atmos. Chem. Phys.*, 15(16),  
603 9285–9312, doi:10.5194/acp-15-9285-2015, 2015.
- 604 Maseyk, K., Berry, J. A., Billesbach, D., Campbell, J. E., Torn, M. S., Zahniser, M. and  
605 Seibt, U.: Sources and sinks of carbonyl sulfide in an agricultural field in the Southern  
606 Great Plains, *Proc. Natl. Acad. Sci.*, 111(25), 9064–9069, doi:10.1073/pnas.1319132111,  
607 2014.
- 608 Monteith, J. L.: Evaporation and environment, in *Symp. Soc. Exp. Biol*, vol. 19, p. 4.,  
609 1965.
- 610 Notholt, J., Kuang, Z., Rinsland, C. P., Toon, G. C., Rex, M., Jones, N., Albrecht, T.,  
611 Deckelmann, H., Krieg, J. and Weinzierl, C.: Enhanced upper tropical tropospheric COS:  
612 Impact on the stratospheric aerosol layer, *Science* (80-. ), 300(5617), 307–310, 2003.
- 613 Parker, G. G., Harmon, M. E., Lefsky, M. A., Chen, J., Pelt, R. Van, Weis, S. B.,  
614 Thomas, S. C., Winner, W. E., Shaw, D. C. and Frankling, J. F.: Three-dimensional  
615 Structure of an Old-growth *Pseudotsuga-Tsuga* Canopy and Its Implications for Radiation  
616 Balance, Microclimate, and Gas Exchange, *Ecosystems*, 7(5), 440–453,  
617 doi:10.1007/s10021-004-0136-5, 2004.
- 618 Paw U, K. T., Falk, M., Suchanek, T. H., Ustin, S. L., Chen, J., Park, Y.-S., Winner, W.  
619 E., Thomas, S. C., Hsiao, T. C., Shaw, R. H., King, T. S., Pyles, R. D., Schroeder, M. and  
620 Matista, A. A.: Carbon Dioxide Exchange between an Old-Growth Forest and the  
621 Atmosphere, *Ecosystems*, 7(5), 513–524, doi:10.1007/s10021-004-0141-8, 2004.
- 622 Protoschill-Krebs, G Wilhelm, C Kesselmeier, J.: Consumption of carbonyl sulphide  
623 (COS) by higher plant carbonic anhydrase (CA), *Atmos. Environ.*, 30(18), 3151–3156  
624 [online] Available from:  
625 <https://www.sciencedirect.com/science/article/pii/S135223109600026X> (Accessed 29



- 626 January 2018), 1996.
- 627 Protoschill-Krebs, G. and Kesselmeier, J.: Enzymatic pathways for the consumption of  
628 carbonyl sulphide (COS) by higher plants, *Bot. Acta*, 105, 206–212 [online] Available  
629 from: <http://onlinelibrary.wiley.com/doi/10.1111/j.1438-8677.1992.tb00288.x/full>  
630 (Accessed 29 January 2018), 1992.
- 631 Sandoval-Soto, L., Stanimirov, M., von Hobe, M., Schmitt, V., Valdes, J., Wild, A. and  
632 Kesselmeier, J.: Global uptake of carbonyl sulfide (COS) by terrestrial vegetation:  
633 Estimates corrected by deposition velocities normalized to the uptake of carbon dioxide,  
634 *Biogeosciences Discuss.*, 2(1), 183–201, doi:10.5194/bgd-2-183-2005, 2005.
- 635 Seibt, U., Kesselmeier, J., Sandoval-Soto, L., Kuhn, U. and Berry, J. A.: A kinetic  
636 analysis of leaf uptake of COS and its relation to transpiration, photosynthesis and carbon  
637 isotope fractionation, *Biogeosciences Discuss.*, 6(1), 333–341, doi:10.5194/bgd-6-9279-  
638 2009, 2010.
- 639 Shaw, D., Franklin, J., Bible, K., Klopatek, J., Freeman, E., Greene, S. and Parker, G.:  
640 Ecological Setting of the Wind River Old-growth Forest, *Ecosystems*, 7(5), 427–439,  
641 doi:10.1007/s10021-004-0135-6, 2004.
- 642 Stimler, K., Nelson, D. and Yakir, D.: High precision measurements of atmospheric  
643 concentrations and plant exchange rates of carbonyl sulfide using mid-IR quantum  
644 cascade laser, *Glob. Chang. Biol.*, 16(9), 2496–2503, doi:10.1111/j.1365-  
645 2486.2009.02088.x, 2010a.
- 646 Stimler, K., Montzka, S. A., Berry, J. A., Rudich, Y. and Yakir, D.: Relationships  
647 between carbonyl sulfide (COS) and CO<sub>2</sub> during leaf gas exchange, *New Phytol.*, 186(4),  
648 869–878, doi:10.1111/j.1469-8137.2010.03218.x, 2010b.
- 649 Sun, W., Maseyk, K., Lett, C. and Seibt, U.: Litter dominates surface fluxes of carbonyl  
650 sulfide in a Californian oak woodland, *J. Geophys. Res. G Biogeosciences*, 121(2), 438–  
651 450, doi:10.1002/2015JG003149, 2016.
- 652 Urban, O., Janouš, D., Acosta, M., Czerný, R., Marková, I., Navrátil, M., Pavelka, M.,  
653 Pokorný, R., Šprtová, M., Zhang, R., Špunda, V. R., Grace, J. and Marek, M. V.:  
654 Ecophysiological controls over the net ecosystem exchange of mountain spruce stand.  
655 Comparison of the response in direct vs. diffuse solar radiation, *Glob. Chang. Biol.*,  
656 13(1), 157–168, doi:10.1111/j.1365-2486.2006.01265.x, 2007.
- 657 Wehr, R., Commane, R., Munger, J. W., Barry Mcmanus, J., Nelson, D. D., Zahniser, M.  
658 S., Saleska, S. R. and Wofsy, S. C.: Dynamics of canopy stomatal conductance,  
659 transpiration, and evaporation in a temperate deciduous forest, validated by carbonyl  
660 sulfide uptake, *Biogeosciences*, 14(2), 389–401, doi:10.5194/bg-14-389-2017, 2017.
- 661 Wharton, S. and Falk, M.: Climate indices strongly influence old-growth forest carbon  
662 exchange, *Environ. Res. Lett.*, 11(4), 1–11, doi:10.1088/1748-9326/11/4/044016, 2016.



- 663 Wharton, S., Falk, M., Bible, K., Schroeder, M. and Paw U, K. T.: Old-growth CO<sub>2</sub> flux  
664 measurements reveal high sensitivity to climate anomalies across seasonal, annual and  
665 decadal time scales, *Agric. For. Meteorol.*, 161, 1–14,  
666 doi:10.1016/j.agrformet.2012.03.007, 2012.
- 667 Whelan, M. E., Hilton, T. W., Berry, J. A., Berkelhammer, M., Desai, A. R. and  
668 Campbell, J. E.: Carbonyl sulfide exchange in soils for better estimates of ecosystem  
669 carbon uptake, *Atmos. Chem. Phys.*, 16(6), 3711–3726, 2016.
- 670 Whelan, M. E., Lennartz, S. T., Gimeno, T. E., Wehr, R., Wohlfahrt, G., Wang, Y.,  
671 Kooijmans, L. M. J., Hilton, T. W., Belviso, S., Peylin, P., Commane, R., Sun, W., Chen,  
672 H., Kuai, L., Mammarella, I., Maseyk, K., Berkelhammer, M., Li, K.-F., Yakir, D.,  
673 Zumkehr, A., Katayama, Y., Ogée, J., Spielmann, F. M., Kitz, F., Rastogi, B.,  
674 Kesselmeier, J., Marshall, J., Erkkilä, K.-M., Wingate, L., Meredith, L. K., He, W., Bunk,  
675 R., Launois, T., Vesala, T., Schmidt, J. A., Fichot, C. G., Seibt, U., Saleska, S., Saltzman,  
676 E. S., Montzka, S. A., Berry, J. A. and Campbell, J. E.: Reviews and Syntheses: Carbonyl  
677 Sulfide as a Multi-scale Tracer for Carbon and Water Cycles, *Biogeosciences Discuss.*,  
678 (October), 1–97, doi:10.5194/bg-2017-427, 2017.
- 679 Winner, W., Thomas, S., Berry, J., Bond, B., Cooper, C., Hinckley, T., Ehleringer, J.,  
680 Fessenden, J., Lamb, B., McCarthy, S., McDowell, N., Phillips, N. and Williams, M.:  
681 Canopy Carbon Gain and Water Use: Analysis of Old-growth Conifers in the Pacific  
682 Northwest, *Ecosystems*, 7(5), 482–497, doi:10.1007/s10021-004-0139-2, 2004.
- 683 Wohlfahrt, G., Brilli, F., Hörtnagl, L., Xu, X., Bingemer, H., Hansel, A. and Loreto, F.:  
684 Carbonyl sulfide (COS) as a tracer for canopy photosynthesis, transpiration and stomatal  
685 conductance: Potential and limitations, *Plant, Cell Environ.*, 35(4), 657–667,  
686 doi:10.1111/j.1365-3040.2011.02451.x, 2012.
- 687 Woodruff, D. R., Mcculloh, K. A., Warren, J. M., Meinzer, F. C. and Lachenbruch, B.:  
688 Impacts of tree height on leaf hydraulic architecture and stomatal control in Douglas-fir,  
689 *Plant, Cell Environ.*, 30(5), 559–569, doi:10.1111/j.1365-3040.2007.01652.x, 2007.
- 690